Molecular Crystals and Liquid Crystals Science and Technology. Section A. Molecular Crystals and Liquid Crystals

Publication details, including instructions for authors and subscription information:
http://www.tandfonline.com/loi/gmcl19

Electronic Structure and Transport Prperties of $AuCl_3$-GIC

Tomohiko Ishil [a] , Yoshihide Komatsu [a] , Kazuya Suzuki [a] , Toshiaki Enoki [a] , Akito Ugawa [b] , Kyuya Yakushi [b] & Shunji Bandow [b]

[a] Department of Chemistry, Faculty of Science, Tokyo Institute of Technology, Okayama, Meguro-ku, Tokyo, 152, Japan

[b] Institute for Molecular Science, Myodaiji, Okazaki, 444, Japan

Version of record first published: 23 Oct 2006.

To cite this article: Tomohiko Ishil , Yoshihide Komatsu , Kazuya Suzuki , Toshiaki Enoki , Akito Ugawa , Kyuya Yakushi & Shunji Bandow (1994): Electronic Structure and Transport Prperties of $AuCl_3$-GIC, Molecular Crystals and Liquid Crystals Science and Technology. Section A. Molecular Crystals and Liquid Crystals, 245:1, 1-6

To link to this article: http://dx.doi.org/10.1080/10587259408051657

Mol. Cryst. Liq. Cryst. 1994, Vol. 245, pp. 1–6
Reprints available directly from the publisher
Photocopying permitted by license only

Printed in the United States of America

ELECTRONIC STRUCTURE AND TRANSPORT PROPERTIES OF $AuCl_3$-GIC

TOMOHIKO ISHII, YOSHIHIDE KOMATSU, KAZUYA SUZUKI, AND TOSHIAKI ENOKI
Department of Chemistry, Faculty of Science, Tokyo Institute of Technology, Ōokayama, Meguro-ku, Tokyo 152, Japan

AKITO UGAWA, KYŪYA YAKUSHI, AND SHUNJI BANDOW
Institute for Molecular Science, Myōdaiji, Okazaki 444, Japan

Abstract We report the optical reflectance, magnetic susceptibility, and magnetoresistance of the first stage $AuCl_3$-GIC which has the shortest c-axis repeat distance among transition metal chloride GICs. The optical reflectance is not explained only in terms of the graphitic π-system. The observed Pauli paramagnetic susceptibility is about three times as large as that from the graphitic π-system. These results suggest the existence of the $AuCl_3$-intercalate band which enhances the density of state at the Fermi energy, although the electrons in the intercalate are more localized than those in the graphitic plane, judging from the magnetoresistance.

INTRODUCTION

Gold trichloride-graphite intercalation compounds ($AuCl_3$-GICs) are formed by the intercalation of dimerized planar molecule Au_2Cl_6. The coplanar arrangement of the Au_2Cl_6 intercalate makes their c-axis repeat distance (d_s=6.86Å) shortest among transition metal chloride-GICs.[1] The intercalate structure is considered to consist of the same planar units Au_2Cl_6 as they are found in pristine Au(III)-chloride,[2] and their in-plane lattice has a $(3\sqrt{3}\times 3\sqrt{3})$R30° superstructure or a $(2\sqrt{7}\times 2\sqrt{7})$R19.1° one depending on a subtle change in composition, which corresponds to $C_{27}(Au_2Cl_6)$ or $C_{28}(Au_2Cl_6)$, respectively. The charge transfer rate and the Fermi energy are estimated by the Raman shift of the graphitic E_{2g2} mode to be $f_c = -0.017$ and $E_F = -0.97$eV, respectively, for the first stage compound, which are relatively large among acceptor-GICs. This suggests the presence of strong electronic coupling between the Au_2Cl_6 intercalate and the graphitic π-system, which is considered to be related to the short c-axis repeat distance and the coplanar intercalate structure. In

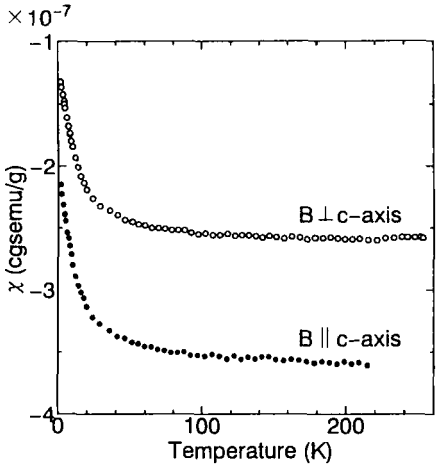

FIGURE 1 : Temperature dependences of magnetic susceptibility of the first stage $AuCl_3$-GIC.

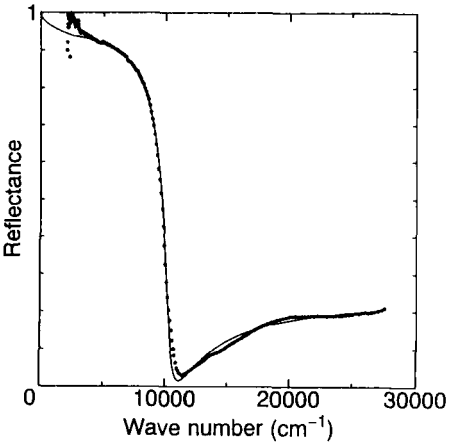

FIGURE 2 : Reflectance data measured at near-normal incidence to the c face of the first stage $AuCl_3$-GIC. The solid line represents the reflectance calculated from the Drude approximation.

this paper, we present the results of the optical reflectance, magnetic susceptibility, and magnetoresistance measurements of the first stage $AuCl_3$-GIC to clarify the electronic properties in relation to the unique intercalate structure.

EXPERIMENTAL RESULTS AND DISCUSSION

i)Magnetic susceptibility

Figure 1 shows the observed susceptibility χ with applied field parallel and perpendicular to the c-axis, which has a negative sign in the whole temperature range. The enhancement χ_{imp} observed at low temperatures below about 40K is associated with the Curie's contribution of lattice defects and impurity which amount is estimated to be 20ppm. The orbital contribution χ_{orb} obtained by subtracting $\chi_\perp$ from $\chi_{||}$ is estimated to be $\chi_{orb} = -0.98\times10^{-7}$cgsemu/g. The negative value of the observed orbital susceptibility is consistent with the theoretical prediction for intraband contribution[3] in the case of the acceptor-type GICs. The Pauli paramagnetic contribution is obtained by subtracting χ_{core}, χ_{imp}, and χ_{orb} from the observed susceptibility, where χ_{core} is the contribution from the core diamagnetism ($\chi_{core} = -5.35\times10^{-7}$cgsemu/g, where the composition of the sample is $C_{14}AuCl_3$). Then, we estimate the observed

Pauli paramagnetic contribution χ_{Pauli} to be 3.0×10^{-7}cgsemu/g.

On the basis of the tight-binding model for the graphitic π-electronic structure, the Pauli paramagnetism $\chi^{\pi}_{\text{Pauli}}$ associated with the π-electrons, which is proportional to the density of state at the Fermi energy, is expressed as follows;

$$\begin{aligned} \chi^{\pi}_{\text{Pauli}} &= 2\mu_B^2 D_\pi(E_F) \quad , \\ D_\pi(E_F) &= \frac{8E_F}{9\pi I_c \gamma_0^2 b^2} \quad (\text{eV}^{-1}\text{cm}^{-3}) \quad , \end{aligned} \tag{1}$$

where I_c, γ_0, and b are the c-axis repeat distance, the in-plane resonance integral, and the in-plane C-C distance (1.42Å). Using eq. (1) and $E_F = -0.97$eV, we obtain the Pauli paramagnetic contribution of the graphitic π-system $\chi^{\pi}_{\text{Pauli}} = 1.1 \times 10^{-7}$cgsemu/g. The observed Pauli paramagnetic contribution is about three times as large as that estimated for the graphitic π-carriers, suggesting the presence of an additional contribution to the Pauli paramagnetism. The enhanced Pauli paramagnetism is considered to be caused by the participation of the $AuCl_3$-intercalate band superposed upon the graphitic π-band.

ii)Optical Reflectance

Figure 2 shows the absolute reflectance at near-normal incidence of the first stage $AuCl_3$-GIC in the photon-energy range 0.31 to 3.4eV, which has a plasma edge at $\sim$10500cm^{-1}. At first, we analyze the reflectance data through fitting only with the Drude approximation, using the following equation;

$$\varepsilon = \varepsilon_c - \frac{\omega_p^2}{\omega(\omega + i\gamma)} \ , \tag{2}$$

where ω_p, γ, and ε_c are the plasma frequency, the relaxation rate, and the core dielectric constant. The parameters are estimated to be $\varepsilon_c = 8.2$ and $\omega_p = 3.66$eV, respectively, after the Kramers-Kronig transformation is made. The theoretical reflectance is indicated by solid line in Fig. 2. On the assumption that only one graphitic π-band contributes to the Drude term, the Fermi energy is estimated by using $\omega_p = 4e^2 E_F/\hbar^2 I_c$ and $I_c = 6.86$Å, that is $E_F = -1.60$eV, which is unrealistically large and significantly different from the value obtained from the Raman spectrum measurement. In order to estimate the Fermi energy correctly, we need the contribution of the interband transition between the graphitic π- and π^*-bands as well as the intraband transition in the analysis in the investigated energy region. The dielectric function is expressed in terms of the Drude-Lorentz model where the

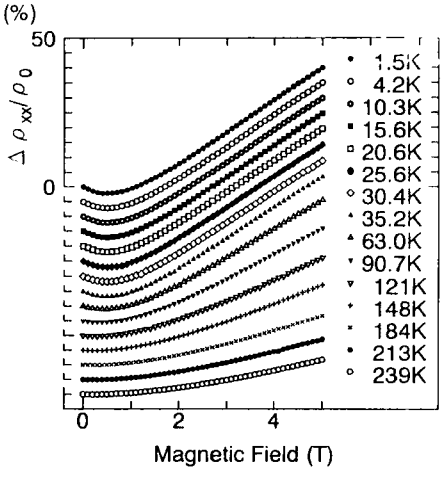

FIGURE 3 : Magnetic field dependence of the magnetoresistance at various temperatures.

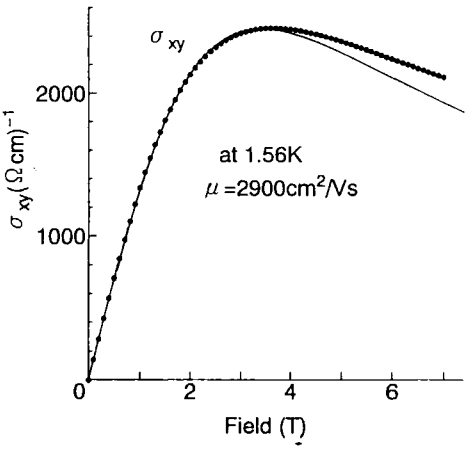

FIGURE 4 : Magnetic field dependence of σ_{xy} of the first stage $AuCl_3$-GICs at 1.5K.

Drude and the Lorentz terms give the contributions of the intraband and the interband transitions, respectively;

$$\varepsilon = \varepsilon_c - \frac{\omega_p^2}{\omega(\omega + i\gamma)} + \frac{f}{(\omega_1^2 - \omega^2) + i\Gamma\omega}\,, \tag{3}$$

where f, ω_1, and Γ are the oscillator strength, the π-π^* energy splitting ($\omega_1 = 2E_F$), and the effective width of the absorption band resulting from the π-π^* transition. After the Kramers-Kronig transformation, a best fitting of the data with eq. (3) is made with the following parameters; $\varepsilon_c = 5$eV, $\omega_p = 3.66$eV, $\gamma = 0.108$eV, and $f = 0.3$. In this analysis, the Fermi energy is also estimated at $E_F = -1.60$eV, which is considerably large in comparison with that obtained by the Raman experiments. The unrealistically large Fermi energy suggests that the analysis on the basis of the graphitic π-bands is not appropriate and an additional contribution from the intercalate bands is required in the optical reflectance.

iii)Magnetoresistance

Figure 3 shows the magnetoresistance of the first stage $AuCl_3$-GIC from 0 to 5T at various temperatures with $I \perp c$-axis and $B \parallel c$-axis. The behavior of the magnetoresistance is described approximately in terms of the one-carrier model since the

magnetoresistance is in proportion to B^2 in the low magnetic field region (B <2T). In the high magnetic field region (B >2T), $\Delta\rho/\rho_0$ has a linear dependence on B. The magnetoresistance reaches 40% of ρ_0 at T = 1.5K and B = 5T. The magnetoresistance decreases as temperature increases, and becomes 25% at T = 80K and B = 5T. Negative magnetoresistance is observed in the low magnetic field region (B <1T) at low temperatures (T <60K), depending on samples. It is considered to be associated with the weak localization of carriers which reflects the random potential in the electronic structure introduced in the intercalation process. This is supported by the large residual resistivity ratio (RRR~3.0) in in-plane resistivity although a resistivity minimum is obscure.

The analysis of the magnetoresistivity ρ_{xx} and the Hall resistivity ρ_{xy} give conductivity tensors σ_{xx} and σ_{xy}. A typical trace of σ_{xy} in the magnetic field is shown in Fig. 4, which can be analyzed approximately in terms of the one-carrier model with hole carriers, although a deviation from the curve predicted by the model appears in the high field region above $4T$. From the experimental data, the mobility of carriers is estimated to be $\mu \sim 2900\text{cm}^2/\text{V}\cdot\text{s}$ at 1.56K, using the following equation;

$$\sigma_{xy} = \frac{ne\mu^2 B}{1+(\mu B)^2}\ , \tag{4}$$

where n is the number of carriers. The relaxation time τ related to the mobility $\mu = e\tau/m^*$, where the effective mass $m^* = 0.16m$ is derived from $E_F = -0.97$eV, is governed by the impurity scattering process τ_i and the phonon scattering process τ_p as given by $1/\tau = 1/\tau_i + 1/\tau_p$. The relaxation times are obtained by fitting of σ_{xx} and σ_{xy}; $\tau_i = 2.4\times10^{-13}$s and $\tau_p = 7.5\times10^{-9}T^{-1.9}$s (1.5K to 240K). The quadratic temperature dependence of $1/\tau_p$ in this temperature region, which is reminiscent of the behaviors in other GICs, suggests a large Debye temperature for in-plane acoustic phonons. The relaxation rate $1/\tau_p$ of the π-carriers at high-temperatures ($T \sim 300$K), where the quadratic temperature dependence becomes less important, is given by[4]

$$\frac{1}{\tau_p} = \frac{D^2 k_B T}{I_c d\hbar v_s^2}\frac{2k}{3\gamma_0 b}\ , \tag{5}$$

where D is a deformation potential for the electron-phonon interaction of the graphitic π-electron with the in-plane acoustic phonon (D = 16eV), d is a density of $AuCl_3$-GIC (d = 3.17g/cm^3), and v_s is a sound velocity of the acoustic phonon ($v_s = 2.1\times10^6$cm/s). Using $k_F \sim 1.4\times10^7\text{cm}^{-1}$ which is given by the Raman spec-

tra, we obtain $\tau_p = 2.8 \times 10^{-13}$s at $T = 300$K. This result is in good agreement with the result obtained from the Hall effect measurement ($\tau_p = 1.5 \times 10^{-13}$s at 300K), and suggests that the graphitic π-electrons govern the in-plane transport process.

SUMMARY

From the magnetoresistance measurement, it is found that the transport property obeys one-carrier model in the first approximation. However, the σ_{xy} data deviate from the fitting curve based on the one carrier model with the graphitic π-hole carriers at high-magnetic fields. This result suggests the presence of the second carriers which are supposed to have too small relaxation time to be observed at low-magnetic fields studied in the present experiment. In addition, the enhanced Pauli paramagnetism suggests the existence of the contribution from the second carriers which are caused by $AuCl_3$-intercalate. Moreover, the observed thermoelectric power in $AuCl_3$-GIC, which is one order of magnitude smaller than that of ordinary acceptor GICs with positive sign, requires the participation of multiple carriers whose contributions are compensated to each other.[5] The intercalate lattice is more disordered than the graphitic plane, resulting in more localized nature of the intercalate electrons. Taking into account the electronic structure established by charge transfer from graphite to $AuCl_3$ intercalate, one concludes that the electronic structure of $AuCl_3$-GICs is described in terms of the superposition of the graphitic π-band and the Au_2Cl_6 intercalate band around the Fermi energy, although the electrons on the intercalate are more localized than those on the graphitic π-plane.

ACKNOWLEDGEMENTS—The authors would like to express their thanks to Dr. A. W. Moore for his generous gift of HOPG. This work is supported partly by Fellowships of the Japan Society for the Promotion of Science for Japanese Junior Scientists, and also partly by Grant-in-Aid for Scientific Research No. 04242103 from the Ministry of Education, Science and Culture, Japan.

REFERENCES

1. R. Vangelisti and A. Hérold, *C. R. Acad. Sci.*, **276 Ser. C**, 1109 (1973).
2. J. Ehrich, P. Behrens, W. Metz, and W. Niemann, *Synth. Met.*, **34**, 217 (1989).
3. R. Saito, *Ph.D. thesis, University of Tokyo*, (1984).
4. K. Sugihara, *Phys. Rev.*, **B 28**, 2157 (1983).
5. T. Ishii, M. Nakao, K. Suzuki, T. Enoki, R. Nishitani, and Y. Nishina, *Solid State Commun.*, **84**, 1055 (1992).